ADVANCED FUNCTIONAL MATERIALS
www.afm-journal.de

A Room-Temperature High-Conductivity Metal Printing Paradigm with Visible-Light Projection Lithography

*Xingyun Yang, Mo Sun, Yinxu Bian, and Ximin He**

Fabricating electronic devices require integrating metallic conductors and polymeric insulators in complex structures. Current metal-patterning methods such as evaporation and laser sintering require vacuum, multistep processes, and high temperature during sintering or postannealing to achieve desirable electrical conductivity, which damages low-temperature polymer substrates. Here reports a facile ecofriendly room-temperature metal printing paradigm using visible-light projection lithography. With a particle-free reactive silver ink, photoinduced redox reaction occurs to form metallic silver within designed illuminated regions through a digital mask on substrate with insignificant temperature change (<4 °C). The patterns exhibit remarkably high conductivity achievable at room temperature (2.4×10^7 S m^{-1}, ≈40% of bulk silver conductivity) after simple room-temperature chemical annealing for 1–2 s. The finest silver trace produced reaches 15 µm. Neither extra thermal energy input nor physical mask is required for the entire fabrication process. Metal patterns were printed on various substrates, including polyethylene terephthalate, polydimethylsiloxane, polyimide, Scotch tape, print paper, Si wafer, glass coverslip, and polystyrene. By changing inks, this paradigm can be extended to print various metals and metal–polymer hybrid structures. This method greatly simplifies the metal-patterning process and expands printability and substrate materials, showing huge potential in fabricating microelectronics with one system.

1. Introduction

The fast development of microelectronics, especially flexible electronic devices (e.g., sensors, displays, and circuits) for new energy, healthcare, and robotic technologies, has boosted the demands for fabricating complex hybrid microstructures comprising both polymeric insulators and metallic conductors in simple processes or even with a single manufacturing system.[1] Fabricating such flexible electronic devices inevitably involves creating conductive metal patterns as the interconnects, heaters, or circuits on low-temperature polymer substrates which are usually heat sensitive, e.g., polyethylene terephthalate (PET) and polycarbonate.[2] However, high temperature up to several hundred degrees Celsius is unavoidably associated with the metal printing processes (e.g., laser sintering) or the post-treatment processes (e.g., thermal annealing) to achieve high conductivity by removing the organic stabilizing agents and sintering the metal particles, which damages the polymer substrates (i.e., deformation or degradation).[3] Additionally, the postannealing using high energy input such as optical sintering and ultrasonic sintering can damage the nanostructure of the as-printed metal patterns when the energy input is exceedingly high.[4] All these local heating issues limit the application of these manufacturing methods on fabricating flexible electronic devices and also hinder the development of emerging technologies, such as "lab-on-skin" electronic devices for real-time health monitoring, which require soft substrates to be mechanically compliant with skins.[5]

Conventional metal deposition methods based on sputtering or evaporation require not only physical masks but also specific cleanroom environment and vacuum condition. Other common metal printing methods, such as inkjet printing,[6] screen printing,[3c] nanoimprinting,[7] and chemisorption printing[8] involve relatively lower fabrication temperature but still require expensive equipment or multistep processes to produce conductive features.[9] Furthermore, it becomes an important trend to manufacture microelectronic devices using a single manufacturing system that is capable of fabricating both inorganic and organic elements. However, since metal and polymer fabrications have different formation mechanisms and processing conditions, directly fabricating both materials with one tool is hard to achieve using most current state-of-the-art methods. Therefore, it is still a grand challenge to develop a simple and universal printing method for fabrication of conductive patterns and hybrid structures at ambient temperature with high electrical conductivity, desirable resolution, and the potential of realizing single-tool device fabrication.

X. Yang, Dr. M. Sun, Dr. Y. Bian, Dr. X. He
Department of Material Science and Engineering
University of California Los Angeles
Los Angeles, CA 90095, USA
E-mail: ximinhe@ucla.edu
Dr. Y. Bian
State Key Laboratory of Modern Optical Instrumentation
Zhejiang University
Hangzhou 310027, China
Dr. X. He
California Nanosystems Institute
Los Angeles, CA 90095, USA
The ORCID identification number(s) for the author(s) of this article can be found under https://doi.org/10.1002/adfm.201807615.

DOI: 10.1002/adfm.201807615

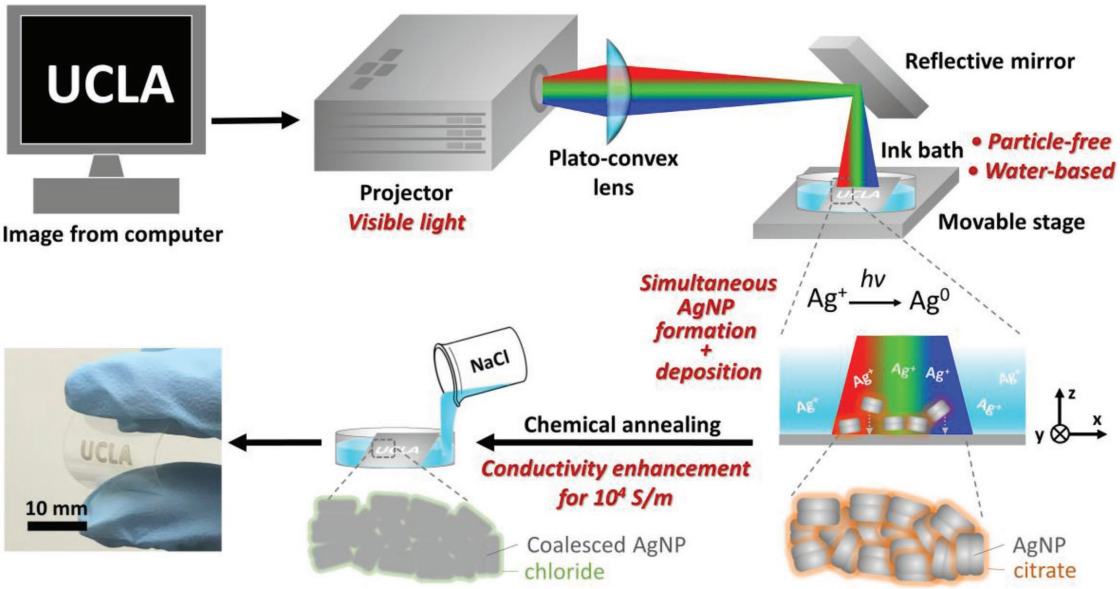

Figure 1. Schematics illustrating the working principle and procedure of the room-temperature Ag printing with visible-light photolithography. A commercial projector projects an exemplary "UCLA"-patterned light through a digital mask on a substrate immersed in the photoreactive silver ink. Silver particles are simultaneously produced and settled on the substrate. Followed by chemical annealing with a NaCl aqueous solution, the conductive Ag pattern of "UCLA" is generated on an exemplary PET substrate shown in the photo.

Here we present a simple and ecofriendly strategy for metal patterning utilizing visible-light-based photolithography under room temperature from a particle-free solution. Highly conductive Ag patterns, with ≈40% electrical conductivity of bulk Ag, are directly printed on various substrates with a high resolution of 15 µm via a commercial projector, as the patterned light through the digital mask from the projector induced chemical reaction transferring Ag^+ in the reactive ink to metallic Ag^0 (**Figure 1**). The entire fabrication process does not require any thermal sintering process and the temperature fluctuation is no more than 4 °C. A particle-free reactive Ag ink, composed of silver nitrate ($AgNO_3$), sodium citrate (Na_3Cit), and sodium nitrate ($NaNO_3$), has been developed with attractive advantages of facile synthesis process and high electrical conductivity for in situ printing metallic Ag on different substrates with easy spatial and temporal control of the pattern formation via photoreduction and at room temperature, which is significantly lower than the printing temperatures of most of the state-of-the-art methods ranging from 80 °C to a few hundreds of degrees Celsius.[1,10] Upon irradiation of white-light digital patterns generated from a commercial available projector, the Ag ink is in situ converted to metallic Ag nanoparticles and simultaneously deposited on the substrates via photoinduced redox reaction with a trivial temperature elevation (less than 4 °C). Each layer of the metallic Ag is fabricated simultaneously as a whole under one light exposure with the finest printed Ag trace of a 15 µm width. The as-printed patterns are then chemically annealed by rinsing with a sodium chloride (NaCl) aqueous solution for a few seconds to remove the capped organic ligands, which effectively enhance the electrical conductivity up to 2.4×10^7 S m^{-1}. This is among the highest level achieved at room temperature[11] and sufficient to serve as conductor in electronic devices. Upon printing and chemical annealing processes, arbitrary conductive Ag patterns with trace width of 15 µm or above can be fabricated (Figure 1). In this method, the whole printing process is conducted in an ambient environment, without vacuum or elevated temperature. The physical mask-free metal patterning technique greatly reduces the number of fabrication steps and simplifies the manufacturing process, which is highly desirable for electronic device industry. This strategy allows for printing metallic patterns on almost all types of substrates, including low-T_g substrates such as PET, rigid substrates such as Si wafer, glass, and polystyrene (PS), and even more flexible materials, such as polyimide (PI), polydimethylsiloxane (PDMS), Scotch Magic tape, and print paper. For the highly conductive Ag patterns fabricated on flexible substrates such as PET, its resistance can change with the extent of deformation, such as bending, which enables it to be used in devices to monitor human breaths or motions. This versatile printing technique is also capable of printing other metals (for example, Pd and Pt) with high performance. It is hoped that this easy metal printing technique can transform the general device manufacturing, by allowing for fabricating traditional and flexible electronics (e.g., ICs, microelectromechanical systems (MEMS), micromirrors, etc.) and prototyping new designs with a single tool in a rapid, low-cost, and high-efficiency manner.

2. Results and Discussion

The projection lithography system that we designed for metal printing consists of a computer, a commercial projector, an optical convex lens, a reflective mirror and a moveable stage (Figure 1). The light of the projector was aligned by the lens and mirror to focus on the substrate immersed in the reactive metal ink bath. The detailed characterization of the light source is

characterized in Figure S1 in the Supporting Information. The light intensity assessed by illuminance could reach 7.7×10^4 lux measured by a digital lux meter. Any arbitrary images or digital patterns can be projected through the projector on a substrate at the focal plane.

To create Ag patterns under visible light at room temperature, we have developed a particle-free photoreactive Ag ink on water basis. In general, the current common inks can be classified into two categories, traditional ink and reactive ink. Traditional ink incorporates metal-based materials with solvent, capping agents, and other additive components. Typical metal-based materials include micro- or nanoparticles, nanorods, nanofibers, and flakes of the zero-valent metal to be sintered subsequently.[10b] Although the traditional ink comprised of Ag flakes has been developed maturely, it requires multiple-layer deposition to make the Ag flakes to overlap to conduct electrons (≈4 µm thick at minimum), leading to resistivity increase.[12] Moreover, its ink preparation involves complicated production and purification of metal particles, making it time consuming and cost inefficient. The particles in the ink are also subject to coagulation when modifiers are added to tune the rheological properties of the ink for better printability.[12] Reactive ink (also known as self-reduced ink) comprises of metal salts dissolved in an appropriate solvent and enables in situ growth of metal patterns via chemical reactions.[10b] Unlike traditional ink that produces loosely connected metal particles in the printed metal patterns, reactive ink could produce high-quality metal structures at relatively lower temperature. Moreover, the preparation process for reactive ink is easier and more convenient than for traditional ink, which requires careful control of reaction parameters, such as temperature, metal salt concentration, and stabilizers.[10b,13] The Ag ink in this work is a reactive ink consisting of $AgNO_3$, Na_3Cit, and $NaNO_3$ in water. It is noteworthy that, compared to the most reported Ag inks using organic solvents, polymers and nanomaterials,[10b] our Ag ink only consists of water and water-soluble salts, which is more stable, environment friendly, and user safe. $AgNO_3$ is the silver source for producing metallic Ag patterns. Na_3Cit serves as a reducing agent for the reduction of Ag^+ to Ag^0 and also a capping agent protecting the formed Ag nuclei from oxidation.[14] $NaNO_3$ enhances the solubility of silver salt due to uncommon ion effect. None of these components and their mixture as the ink exhibit absorbance at around 400 nm, which proves that there are no Ag nanoparticles existing in the Ag ink used for printing (Figure S2, Supporting Information).[15] Upon white light irradiation, a photoinduced redox reaction occurs, transforming Ag^+ to Ag^0 due to the electron transferring between Cit^{3-} and Ag^+. After printing, the pattern was chemical annealed by simply rinsing the substrates with a 20×10^{-3} M NaCl aqueous solution, leading to the Ag pattern change from dark colored to metallic bright and mirror-like appearance (**Figure 2**a). Comparing to other metal patterning methods, the visible-light projection lithography technique reported in this work greatly simplified the metal patterning processes and brought down the fabrication temperature to room temperature. In conventional metal deposition with photolithography processes, each conductive pattern of different design requires making a different physical mask, which complicates the fabrication process and increases both the material cost and the fabrication time. Also, inkjet printings using nanoparticle-polymer inks is sensitive to ink formulation (particle size and loading) leading to nozzle clogging issues and only operates under a narrow range of ink viscosity (<100 cP).[9e] The metal nanoparticle powders used in laser-based printing involve contamination issues and health concerns due to the risk of inhaling nanomaterials.[16] Hence, this presented inexpensive and ecofriendly projection lithography metal pattern manufacturing technique is highly advantageous and owns broad impacts in transforming the manufacturing of many different devices.

The printed Ag pattern exhibited a high electrical conductivity of 2.4×10^7 S m^{-1} after chemical annealing at room temperature, which corresponded to ≈40% of the bulk Ag conductivity. Usually a high processing or postannealing temperature is required to obtain a high conductivity of printed Ag patterns. Lower fabrication temperature will result in insufficient interconnection between metal particles and thus a less satisfactory conductivity. It is always a challenge to produce arbitrary metal patterns with desirable conductivity while keeping the manufacturing temperature low. With this simple printing method, the Ag patterns fabricated at low temperature possess a remarkably high electrical conductivity, in comparison with other reported Ag patterning methods (Figure 2b and Table S1, Supporting Information). This is attributed to initial close packing of the as-produced Ag particles on the substrate and more to the subsequent chemical annealing with NaCl, which significantly increased the packing and thus the conductivity further for four orders of magnitude, from the initial 3.2×10^3 S m^{-1} before annealing, as shown in Figure 2a. In details, the introduction of Cl^- via NaCl rinsing induces the desorption of capping agent (Cit^{3-}) from the surface of as-printed metallic Ag particles and brings the Ag particles into contact and coalescence,[17] so that more percolation paths for electron transport are generated and an interconnected network is formed. The scanning electron microscopy (SEM) images of Ag samples before and after chemical annealing (Figure 2c) proved that after treated by NaCl, Ag particles coalesced to form necks and generated continuous metal network. While other kinds of halides, such as NaF, NaBr, NaI, KCl, $CaCl_2$, and HCl, which have strong interactions with Ag, can also effectively remove stabilizers from Ag surfaces and greatly increase the conductivity,[17,18] we use NaCl in this work for its low cost and environmental friendliness, which is beneficial for future commercial applications. Additionally, the chemical annealing is a fast process that occurs immediately upon the addition of NaCl without any additional thermal energy input. Thus this room-temperature sintering strategy could significantly enhance the electrical conductivity of the printed Ag samples by four orders of magnitude in a few seconds, without the expenses of laser and destroying the heat-sensitive substrates.

In order to investigate the parameters and obtain an optimal Ag ink recipe, we then varied the concentration of each component in the Ag ink. First, the influence of citrate concentration was studied by fixing irradiation time at 15 min and the $AgNO_3$ and $NaNO_3$ concentration at 10×10^{-3} and 150×10^{-3} M, respectively, while changing the concentration ratio [Na_3Cit]/[$AgNO_3$] from 0.5, 1, 1.5, 2, 2.5 to 5. The patterns were printed on a flexible PET film and chemically annealed by NaCl. As the

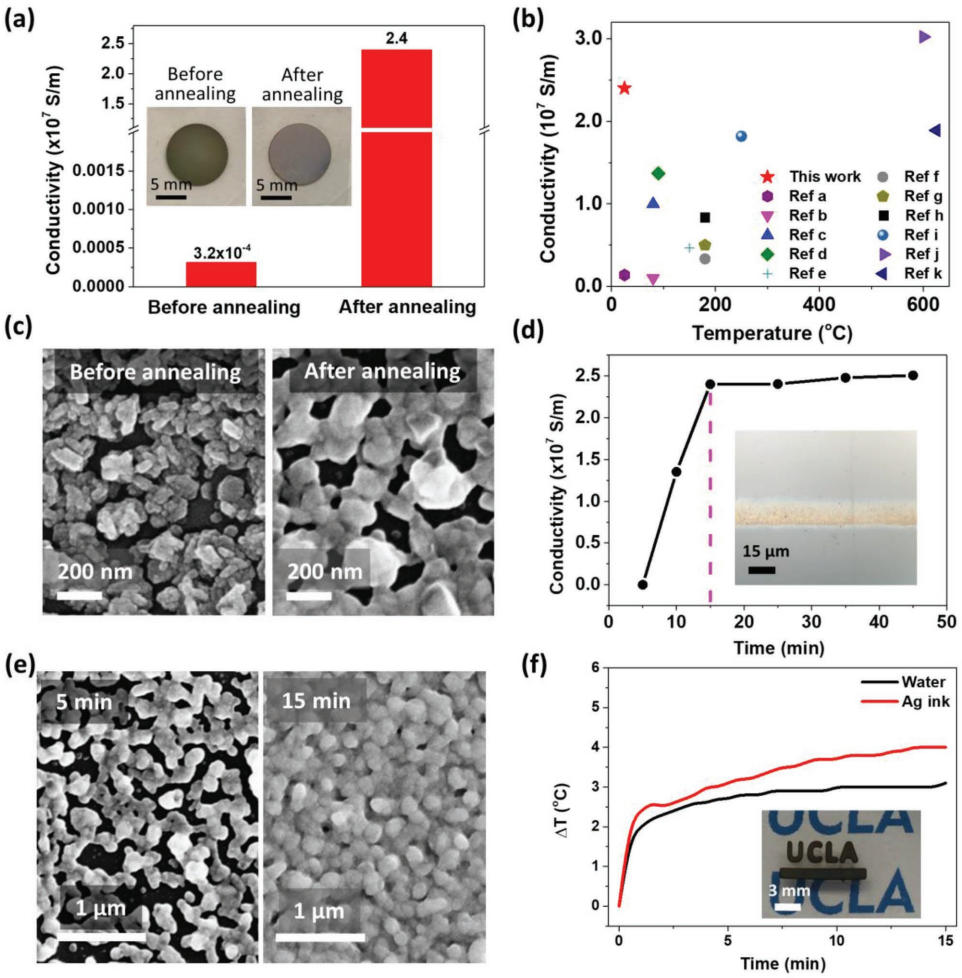

Figure 2. a) Electrical conductivity of Ag samples on PET substrate (irradiation time = 15 min) before and after chemical annealing (at room temperature). (Inset) Photographs of Ag patterns on PET substrate before and after chemical annealing using a 20×10^{-3} M NaCl aqueous solution. b) Comparison of the conductivity and processing temperature of our Ag printing technique and other reported methods. Ref a,[11b] b,[1] c,[8] d,[13] e,[3c] f,[21] g,[22] h,[12] i,[3b] j,[23] k.[3a] c) SEM images of Ag samples obtained without and with chemical annealing. For the two samples, the irradiation time was 5 min in order to clearly show the morphology of particles and the formation of necking. d) Conductivity of Ag samples on PET substrate after chemical annealing as a function of concentration ratio $[Na_3Cit]/[AgNO_3]$. The Ag ink comprised of 10×10^{-3} M $AgNO_3$, 150×10^{-3} M $NaNO_3$, and various concentration of Na_3Cit (irradiation time = 15 min). (Inset) Optical microscopy image of Ag trance printed on PET substrate to show the smallest width could be produced reached 15 μm. e) SEM images of Ag samples with 5 and 15 min irradiation. f) Normalized temperature profile as a function of irradiation time for Ag printing with optimized Ag ink recipe. For comparison, the Ag ink is replaced with deionized water and the normalized temperature profile for water under the same conditions is recorded. (Inset) Photograph of Ag sample printed on poly(*N*-isopropylacrylamide) with a lower critical solution temperature (LCST) of 32 °C. The polymer substrate remained transparent and did not shrink throughout the whole printing process.

concentration ratio $[Na_3Cit]/[AgNO_3]$ increased, the conductivity first increased and then decreased (Figure S3, Supporting Information), with the highest conductivity of 2.4×10^7 S m^{-1} located at $[Na_3Cit]/[AgNO_3]$ = 1.5. Their corresponding SEM images were shown in Figure S4 in the Supporting Information. Based on this, we fixed the concentration ratio $[Na_3Cit]/[AgNO_3]$ at 1.5 and further tuned the concentration of other components. Next, we studied the influence of $AgNO_3$ concentration by fixing the irradiation time at 15 min, concentration ratio $[Na_3Cit]/[AgNO_3]$ at 1.5 and $NaNO_3$ concentration at 0 M, while changing the concentration of $AgNO_3$ from 5×10^{-3}, 10×10^{-3} to 15×10^{-3} M. At first, we expected higher concentration of $AgNO_3$ would be beneficial for the conductivity of printed Ag samples. However, the conductivity results for $[AgNO_3] = 5 \times 10^{-3}$, 10×10^{-3}, and 15×10^{-3} M were 0.27×10^7, 1.9×10^7, and 1.5×10^7 S m^{-1}, respectively, with the best conductivity result located at $[AgNO_3] = 10 \times 10^{-3}$ M (Figure S5, Supporting Information). This could be explained by the limited solubility of silver citrate. When mixing $AgNO_3$ and Na_3Cit, silver citrate was formed with a water solubility as low as 0.0285 g L^{-1}.[14] With increasing $AgNO_3$ concentration, the ink became white and turbid due to the undissolved silver citrate. This suspension ink would scatter the light, and lower the efficiency of the redox reaction, so that less metallic Ag was produced in a fixed time course and finally caused a lower conductivity of the printed Ag samples. To solve this problem, $NaNO_3$ was added to the ink to increase the solubility of silver citrate due to uncommon ion effect. While changing the concentration ratio $[NaNO_3]/[AgNO_3]$

from 0, 5, 10, 15 to 20, the other conditions remained the same, i.e., irradiation time = 15 min, $[AgNO_3] = 10 \times 10^{-3}$ M, and $[Na_3Cit] = 15 \times 10^{-3}$ M ($[Na_3Cit]/[AgNO_3] = 1.5$). As shown in Figure S6 in the Supporting Information, the solutions changed from white and turbid to transparent and the transmittance increased with higher concentration ratio $[NaNO_3]/[AgNO_3]$. The conductivity of printed Ag samples after chemical annealing as a function of concentration ratio $[NaNO_3]/[AgNO_3]$ was plotted in Figure S5 in the Supporting Information. As $[NaNO_3]/[AgNO_3]$ increased, the conductivity first increased and then decreased with the highest conductivity of 2.4×10^7 S m^{-1} located at $[NaNO_3]/[AgNO_3] = 15$. Another important role of $NaNO_3$ was to assist the deposition of generated metallic Ag particles onto the substrate, which was verified by collecting the Ag ink after the printing process and measuring its UV–vis absorption spectra. Figure S7 in the Supporting Information showed the UV–vis absorption spectra of Ag inks with different value of $[NaNO_3]/[AgNO_3]$ after a 15 min irradiation. Without addition of $NaNO_3$ ($[NaNO_3]/[AgNO_3] = 0$), an absorption peak appeared at around 430 nm, corresponding to the formed Ag particles upon light irradiation. However, no significant absorption at 430 nm was observed for the Ag inks when $NaNO_3$ was added ($[NaNO_3]/[AgNO_3] = 5$, 10, 15). This indicated that the photon-induced generated Ag particles deposited onto the substrate rather than suspended in the solution. The addition of $NaNO_3$ increased the electrolyte concentration in the system, resulting in the compression of the Stern layer and a decrease of zeta potential, and thus the formed Ag nanoparticles tended to flocculate rather than to suspend in the solution.[19] Overall, the optimal Ag ink formulation was comprised of 10×10^{-3} M $AgNO_3$, 15×10^{-3} M Na_3Cit, and 150×10^{-3} M $NaNO_3$.

With this optimized Ag ink recipe, we investigated the effect of printing time on the conductivity of printed Ag patterns. Figure 2d shows the conductivity of Ag patterns on PET substrate after chemical annealing as a function of time. The conductivity first increased and then reached a plateau as irradiation time increased. Although clear Ag patterns were generated with only 5 min irradiation, the patterns were not conductive. As shown in the SEM image (Figure 2e) for the Ag sample with 5 min irradiation, not enough Ag particles generated to cover all the area of light irradiation and many microvoids lay between the Ag clusters and prevented them from connecting to each other. The conductivity of the Ag patterns increased to 1.4×10^7 S m^{-1} when irradiated for 10 min and reached a plateau value of 2.4×10^7 S m^{-1} with 15 min irradiation. From the SEM images shown in Figure 2e and Figure S8 in the Supporting Information, we found that with longer irradiation time (15–45 min), the generated Ag particles nearly covered all the area of irradiation and denser structures with no significant microvoids formed, which explained the excellent electrical performance of the printed Ag patterns from microscopic aspect. Based on the above results, our method can produce highly conductive Ag patterns with a scale of 2×3 cm^2 in only 15 min, which could have potential applications for rigid and flexible electronic devices. The finest Ag traces we fabricated reached 15 μm (Figure 2d, inset), yet the Ag traces could be further scaled down by utilizing higher resolution projector.

We conducted detailed studies of the manufacturing temperature, proving that the whole process is conducted under room temperature. The temperature change during the printing process was measured by a temperature controller. The normalized temperature profile during printing is recorded in Figure 2f and a comparison with irradiation on deionized (DI) water under the same conditions was recorded as the reference. In the first 2 min, both the temperatures of the Ag ink and water had a sudden increase for about 2.5 °C originating from projector irradiation. Then for 15 min irradiation, temperature elevation in water was 3.1 °C while in Ag ink solution was 4.0 °C. The higher temperature elevation in the Ag ink than in water resulted from the photoinduced redox reaction converting Ag^+ to Ag^0 in the ink bath. During the time course of Ag printing (15 min), the total temperature increasing was no more than 4.0 °C and the tiny temperature elevation was bearable for most of the flexible plastic substrates. As shown in Figure 2f, inset, Ag was printed on a temperature-sensitive polymer substrate, poly(*N*-isopropylacrylamide), which would contract and turn opaque upon heating up to around 32 °C,[20] serving as a local temperature indicator here. The polymer substrate remained transparent and did not shrink throughout the whole printing process, which further proved the low processing temperature of our metal printing technique. Therefore, this room-temperature strategy for Ag patterning has great potential for printing patterns on various low-melting-temperature materials and biological surfaces.

This technique exhibits a high versatility in terms of compatible substrates, printable structures, and materials. Specifically, here we show its great compatibility with various substrates, the easiness of printing different patterns and 3D structures, and its suitability of printing organic–inorganic hybrid patterns and different metals. To demonstrate the compatibility with various substrates, we fabricated Ag patterns on several kinds of substrates, including rigid substrates, such as Si wafer, glass cover slip, polystyrene, and also flexible substrates, such as PET, PDMS, polyimide thin film, Scotch Magic tape, and print paper (**Figure 3**a–h). Highly conductive Ag patterns were successfully produced on all the above substrates, which proved its general applicability to a wide variety of substrates. Especially, neither of the printing process nor the post-treatment involved high-temperature steps, which enabled this method to print patterns on heat-sensitive substrates, for example, polymers and other organic materials. Since the patterns are projected by commercial projectors or digital light processing systems, this system can print almost all forms of digital images of arbitrary characters and graphic designs conveniently. As shown in Figure 3a–h, the University of California Los Angeles (UCLA) logo, a mesh structure, a circuit pattern, and a fan shape were printed. Energy-dispersive X-ray spectroscopy (EDS) analysis results of these printed Ag patterns (≈90 nm thick) were presented in Figure S9 and Table S2 in the Supporting Information. Due to the low thickness of the Ag layer (≈90 nm), the excitation source used for elemental analysis penetrated the thin Ag layer and reached the substrate, which gave the chemical characterization of both the Ag layer and the PET substrate. The quantitative EDS results of selected area of the printed Ag and the PET substrate exhibited similar weight ratio of oxygen to carbon (O wt%/C wt% = 2.8 and 2.7 for Ag region and PET region, respectively), indicating a high purity of printed Ag with nearly no impurities such as silver oxide. The carbon and

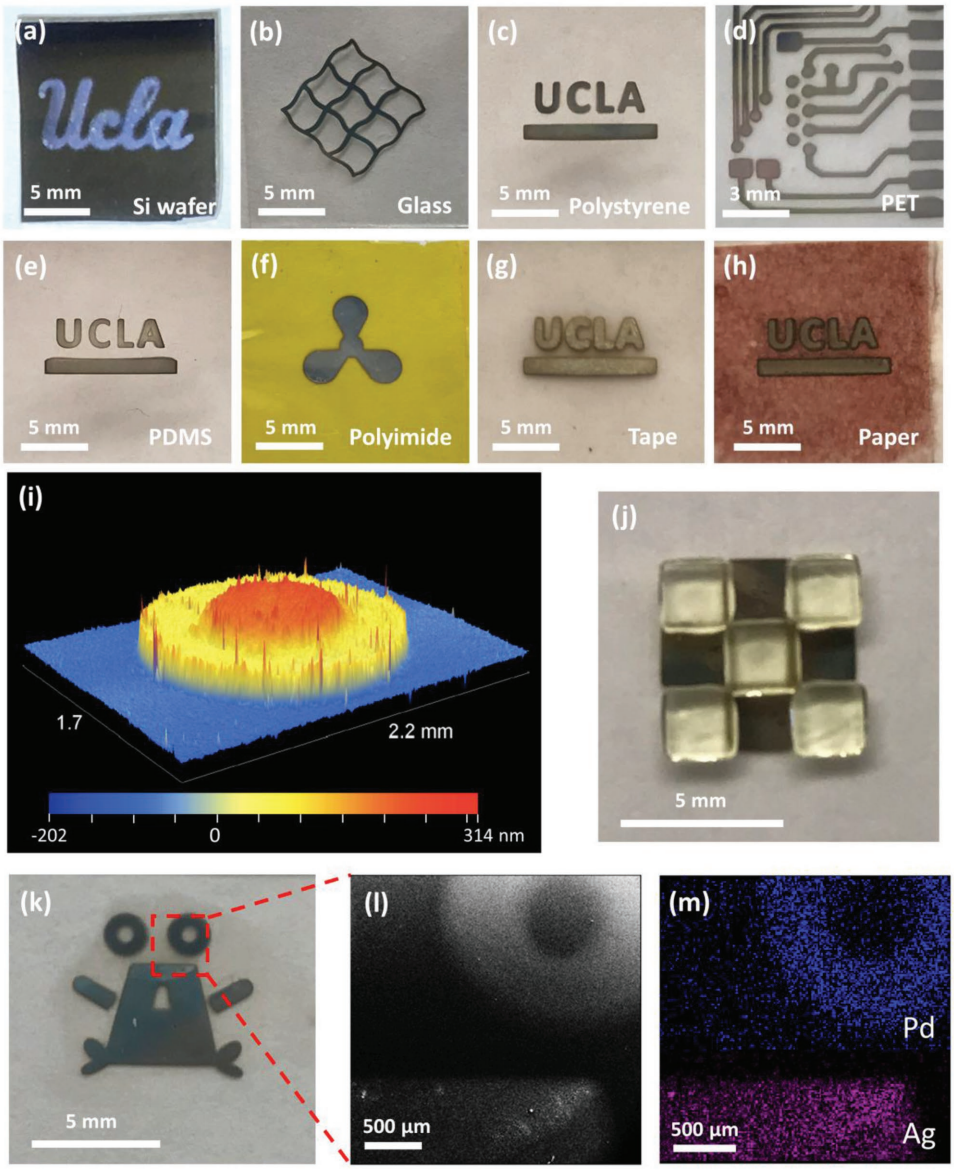

Figure 3. Photograph of printed Ag patterns on various substrates, a) Si wafer, b) glass cover slip, c) polystyrene, d) PET, e) PDMS, f) polyimide, g) Scotch Magic tape, h) print paper. i) 3D surface topography of a two-layer structure printed on Si wafer measured by optical profiler. j) Photograph of a checkerboard made of poly(1,6-hexanediol diacrylate) (yellow) and silver (gray). k) Photograph of a frog printed with Pd (eyes) and Ag (body). l) SEM image of part of the printed frog. m) EDS image map indicating the region of Pd and Ag.

oxygen signal from the printed Ag region originated from the PET substrate.

Such a diversity of arbitrary and complex patterns demonstrated here showcases the important advantage of this on-demand (temporal) and remotely controlled (spatial) photoreduction of this novel photoreactive silver ink. Such a function cannot be achieved by many other reactive inks such as Tollens' reagent. Since Tollen's reagent instantly forms silver particles upon mixing with the reducing agents, silver patterning with this ink requires complex design of multiple microfluidic channels, including separate reagent inlet channels merging into the main microreactor channel of predesigned pattern, which guides the silver particle deposition to form a silver pattern that is determined by the channel design.[11d] By contract, the photoreactive ink developed in this work does not require physical mask or channel, making the printing system design extremely simple.

We further show the benefit of such a reactive ink-based photolithography by simply lowering the sample stage to stack the printed metal layer by layer into a 3D structure. An exemplary two-layer stereoscopic silver structure was printed on Si wafer, shown by the optical profilometry image (Figure 3i), with a height difference between two layers of ≈140 nm. This demonstrated the potential of this stereolithographic method in printing 3D structures. We also used this system to print organic–inorganic hybrid materials and other metals. As shown in Figure 3j, a checkerboard pattern consisted of silver and poly(1,6-hexanediol diacrylate) (pHDDA) was fabricated

with a single manufacturing system. The pHDDA was printed with the same apparatus as was the Ag component, by simple changing the solution to corresponding polymer precursor. Beyond printing Ag, Figure 3k,l shows a frog pattern printed of palladium (Pd) for the eyes and Ag for the body. The element mapping image by EDS (Figure 3m) confirmed high purity and clear spatial distinction of the different metals. This demonstrates that, with appropriate photoreactive inks, this technique possesses the potential to print more complicated patterns and structures comprising of different materials. Overall, the above arbitrary patterns printed of different metals and polymers on various substrates showcase the generality and powerfulness of this platform.

We also explored the unique resistance tunability upon bending and the flex stability after cyclic mechanical deformation of the flexible silver patterns. Ag electrodes (≈90 nm thickness) were printed on a soft PET substrate (100 µm thick) and their electrical resistance changes upon outward and inward bending, respectively, were tested. By bending the sample outward at different bending radius from 22.9 mm down to 0.1 mm (fully folded), the electrical resistance can be well controllably tuned to increase (R/R_0 increased from 1.05 to 2.62) with the bending radius decrease (**Figure 4**a), since microvoids and cracks form in the Ag electrode under tensile strain. Alternatively, by bending the sample inward, the electrical resistance decreased (R/R_0 decreased from 1.00 to 0.72) with bending radius decrease, since the compression strain led to denser particles packing. When the silver patterns were flattened after bending, the resistance could recover to the original state. The resistance of the silver patterns stayed constant for

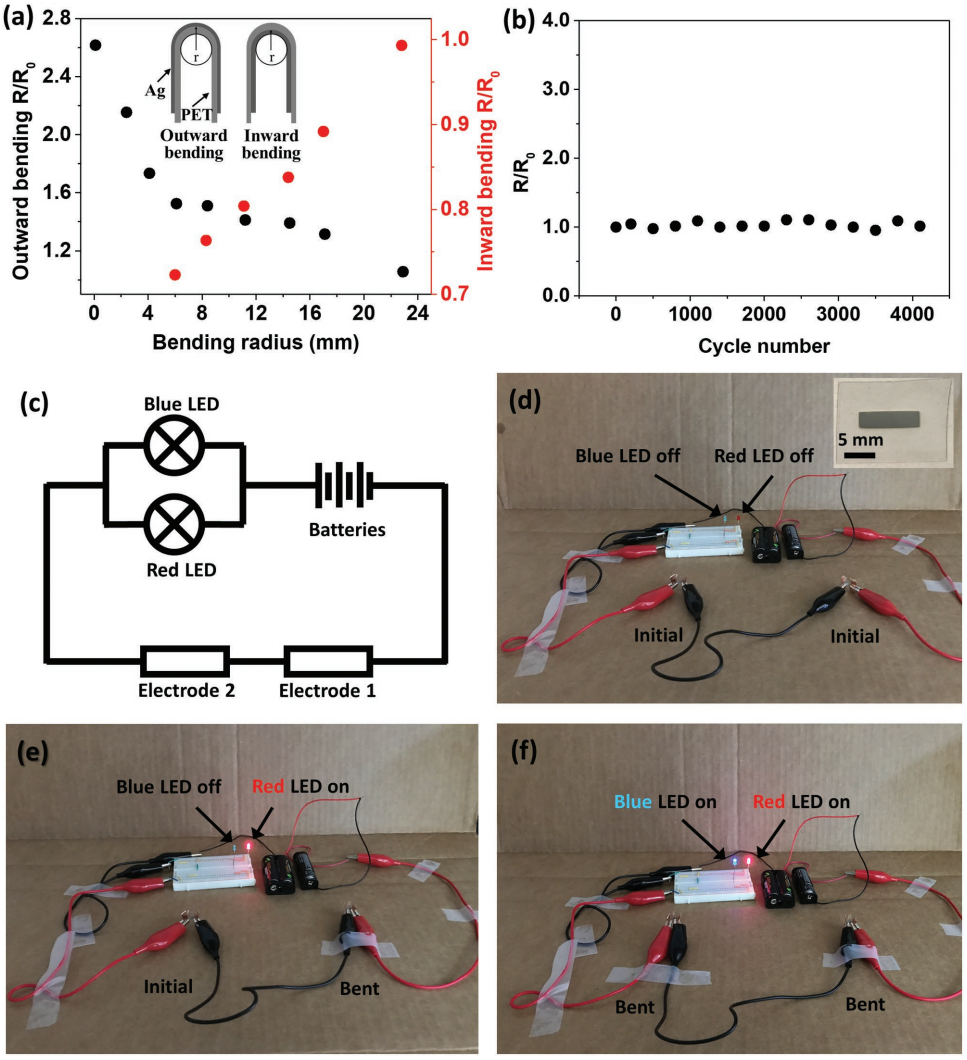

Figure 4. a) Resistance tunability of the printed flexible Ag electrodes on PET substrate by changing the bending radius. (Inset) Schematic diagram for outward and inward bending of the Ag-PET film. b) Fatigue test of printed Ag electrodes on PET substrate measured by resistance change upon outward bending as a function of bending cycle number at bending radius = 7.7 mm. c) Circuit design of a logic gate device fabricated with printed Ag electrodes on PET substrate. The two LED bulbs (represented by a circle with cross inside) were connected in parallel, while the two printed Ag electrodes (represented by rectangle) were connected in series. (Insect) Photograph of the electrode used in the device. d) When both electrodes were not bended, neither LED bulb was on. e) Only one electrode was bended, the red LED was on while the blue LED remained off. f) When both electrodes were bended, both red and blue LEDs were on.

4000 cycles of repetitive outward bending at 7.7 mm bending radius (Figure 4b). This demonstrates excellent fatigue resistance.

Because of the excellent resistance tunability and fatigue resistance, the printed Ag pattern can be readily used in strain sensors, flexible circuits, wearable electronics, and biomedical devices. To demonstrate its application, we fabricated a simple logic gate device by integrating the printed Ag electrodes on a PET substrate with light-emitting diodes (LEDs) and control the on and off of the LEDs by tuning conductivity of the Ag electrodes via bending. The circuit diagram design is shown in Figure 4c. Two LED bulbs (red and blue) were connected in parallel, while the two printed Ag electrodes on PET substrate were connected in series. Utilizing the forward voltage difference between the red (2.05 V) and blue (3.5 V) LED bulbs, the on/off of the LED bulbs could be controlled by adjusting the voltage partition in the circuit. Since the bending of electrodes induced a resistance change in the circuit, the voltage partition could be easily adjusted through bending one or both of the two electrodes and thus the on/off of the LED bulbs could be manipulated. When both electrodes were at initial state (Figure 4d and Movie S1, Supporting Information), the system had large resistance and both red and blue LED bulbs were off. When one electrode was bended inwardly and other one was still in initial state, resistance decreased to medium level and only the red LED bulb was on (Figure 4e). When both electrodes were bended inwardly, the resistance decreased further to a low level and both red and blue LED bulbs gained enough voltage to be turned on (Figure 4f). Since our technique is able to create conductive Ag patterns on flexible substrates without any thermally induced damage, it shows potential to be fabricated into electronic skins and soft electronics, for example, soft robots and wearable devices to monitor the breath or bending of joints for health or diagnosis purpose.

3. Conclusion

In summary, we report a new room-temperature, visible-light projection lithography technique for fabricating highly electrically conductive Ag patterns on various substrates including flexible and rigid ones. This technique utilizes photosensitive Ag reactive ink to achieve Ag patterning through a chemical approach and leads to a high electrical conductivity of the printed Ag patterns, 2.4×10^7 S m^{-1}, around 40% of the conductivity of the bulk silver, outperforming most current metal printing methods. No significant temperature elevation during Ag printing process is observed, which greatly extends the choice for substrates. This especially allows for the usage of many low-temperature substrates that otherwise cannot used by conventional metal manufacturing methods, opening up the opportunities for many unprecedented functions of novel devices. Moreover, this design greatly simplifies the fabrication processes of metal patterns, avoiding expensive equipment, vacuum conditions, high manufacturing temperature, and multiple-step processes in conventional metal patterning methods, and it also brings down the cost and time for metal printing. Furthermore, by choosing appropriate photoreactive inks, the technique can be further extended to print metals beyond Ag and metal–polymer hybrid materials with exactly the same apparatus, such as Pd, and pHDDA-Ag hybrid structures. Beyond 2D patterns, this technique is also capable of fabricating stereoscopic objects, demonstrating the potential to manufacture 3D printing structures. Overall, this is a facile and convenient technique to achieve high-quality metal and polymer patterning with simple apparatus setup and easy-synthesized reactive ink, which at the same time avoids high processing temperature, expensive equipment, and harsh experimental conditions.

4. Experimental Section

Materials: Silver nitrate ($AgNO_3$, >99.7%), sodium citrate dihydrate ($Na_3C_6H_5O_7{\cdot}2H_2O$, 99.0%), sodium nitrate ($NaNO_3$, >99%), sodium chloride (NaCl, >99.0%), toluene ($C_6H_5CH_3$, >99.5%), methanol (CH_3OH, >99.8%), and petri dishes (PS) were purchased from Fisher Scientific. Ammonium iron(III) oxalate trihydrate ($(NH_4)_3[Fe(C_2O_4)_3]{\cdot}3H_2O$, 98%) and poly(dimethylsiloxane) (PDMS prepolymer, Sylgard 184) were purchased from ACROS Organics. Ammonium tetrachloropalladate(II) [$(NH_4)_2PdCl_4$, 99.998%] was purchased from Alfa Aesar. (3-Aminopropyl) triethoxysilane (APTES, >98%), 1,6-hexanediol diacrylate (HDDA, 80%), PET film (0.1 mm thickness), and PI (0.008 mm thickness) were purchased from Sigma-Aldrich. Scotch Magic tape and inkjet print paper were purchased from Office Depot. All chemicals were used as received without further purification.

Silver (Ag) Ink Preparation: The Ag ink was prepared by mixing the silver nitrate ($AgNO_3$), sodium citrate (Na_3Cit), and sodium nitrate ($NaNO_3$) solutions to expected final concentrations. All the concentrations mentioned in this work referred to the final concentration of the corresponding compound in Ag ink. In a typical Ag ink preparation process, 1 mL of 100×10^{-3} M $AgNO_3$ was mixed with 1 mL of 150×10^{-3} M Na_3Cit solution, 1 mL of 1500×10^{-3} M $NaNO_3$ solution, and 7 mL deionized water to give a final Ag ink comprised of 10×10^{-3} M $AgNO_3$, 15×10^{-3} M Na_3Cit, and 150×10^{-3} M $NaNO_3$. DI water was ultrasonic degassed for 30 min before using to prepare all the solutions.

Palladium (Pd) Ink Preparation: The Pd ink was prepared following the recipe reported by Zarzat et al.[24] In brief, aqueous solution 0.7 M of $(NH_4)_2[PdCl_4]$ and 1 M of $(NH_4)_3[Fe(C_2O_4)_3]{\cdot}3H_2O$ were prepared and stored in dark. The two solutions were mixed in 1:1 volume ratio before printing.

Surface Modification: No surface modification was needed for most of the substrates used in this work, including PET, glass, polystyrene, polyimide, Scotch Magic tape, and print paper. However, surface modification was required to enhance the affinity of Si wafer and PDMS to the formed Ag particles. The surface modification of Si wafer was conducted based on the work from Luo and co-workers.[25] In brief, the Si wafer was first treated by pure oxygen plasma (Harrick Plasma, PlasmaFlo PDC-FMG and Plasma cleaner PDC-001) at 750 mTorr for 3 min to introduce hydroxyl groups to the surface. Next, the Si wafer was immersed in 3×10^{-3} M APTES toluene solution for 6 h to introduce the APTES aminosilanization film. Then the Si wafer was rinsed with pure toluene, toluene, and methanol mixture (1:1 in volume), and pure methanol in sequence. Finally, the Si wafer was dried with air flow. The surface modification of PDMS was conducted based on the work from Cho and co-workers.[26] In brief, the PDMS was first treated by pure oxygen plasma at 750 mTorr for 3 min to introduce hydroxyl groups to the surface. Then the PDMS was immersed in 1% v/v aqueous APTES solution for 20 min. Finally, the PDMS was rinsed with DI water and following by drying with air flow.

Photolithography System: The system constituted of three major components: a commercially available projector (BenQ MH530) providing patterned light source in the range of visible light; converging lens with the focal length of 60.0 mm (Thorlabs LA1401-A) and reflective mirror (Thorlabs ME2S-P01) to focus and align the light path, respectively; and a movable stage used to place the holder for ink bath.

All the optics and the movable stage were purchased from Thorlabs Inc. A substrate was fixed in the holder (Petri dish) containing Ag ink with the solution depth of 2–3 mm. The spectrum of the light source was measured using a UV–vis spectrometer (Thorlabs CCS200).

Ag Patterning: The light patterns could be conveniently generated by commercial available software such as Microsoft Power Point and be projected onto the substrate. The substrate was fixed on the holder and placed on the movable stage. The height of the stage was tuned to ensure the light patterns focusing on the upper surface of the substrate. Then the light path was blocked with a paper board and silver ink was poured into the holder to make sure the substrate was totally immersed in the solution. After that the paper board was removed. As soon as the light irradiated on the substrate, the silver ink began to decompose to generate metallic silver at irradiated areas.

Chemical Annealing: After a printing cycle, the substrate with the printed silver patterns on it was rinsed with DI water for three times to remove the remained silver ink. Then the substrate was rinsed with 20×10^{-3} M NaCl solution for 1–2 s to carry out chemical annealing. Next, the sample was rinsed with DI water again for three times to remove the remained sodium chloride. At last, the printed sample was air dried.

Resistivity Measurement: Thin circle films of Ag sample with diameter of 1 cm were printed for resistivity measurement. After chemical annealing with NaCl solution, the thickness of the sample was measured using an optical profiler (Bruker NT9300 Optical Profiler). Electrical resistance measurements were acquired using a four-point resistance probe (Jandel, CYL-1.0-60-TC-100-1M) connected to a source meter (Keithley 2400, Keithley Instruments, Inc.).

Characterization of Ag Ink: The UV–vis absorption spectrum and transmittance spectrum of the Ag ink is obtained using a UV–vis spectrometer (Ocean Optics USB2000+) with a standard 1 cm liquid cuvette.

Characterization of Printed Ag Patterns: SEM is used to image the surface of Ag patterns printed on various substrates. The SEM images are acquired using a field emission microscope (ZEISS Supra 40VP SEM). This instrument was equipped with Thermo Noran System SIX EDS system, which was used for elemental analysis for a multimetal printed sample comprised of Ag and Pd.

Temperature Measurement: The temperature profile during the reaction was obtained by a temperature controller (WILLHI WH1436A). The thermal sensor probe was placed at the light irradiated area and was totally immersed into the solution as the printing processing.

Logic Gate Device Design and Components: A logic gate device was fabricated by connecting 1 red LED (Kingbright, WP7113ND) and 1 blue LED (Visual Communications Company, VAOL-3LSBY2) in parallel and two printed Ag electrodes in series. Each electrode was fabricated in the dimension of 1 cm × 0.25 cm.

Supporting Information

Supporting Information is available from the Wiley Online Library or from the author.

Acknowledgements

X.Y. and M.S. contributed equally to this work. The authors thank the valuable discussion and technical supports from Zach Ballard and Dr. Aydogan Ozcan from UCLA. X.H. acknowledges the UCLA start-up funding, UCLA faculty career development award, Office of Naval Research (ONR) award (N00014-17-1-2117), and ONR Defense University Research Instrumentation Program (DURIP) award.

Conflict of Interest

The authors declare no conflict of interest.

Keywords

flexible electronics, high conductivity, hybrid material printing, metal patterning, room-temperature printing

Received: October 26, 2018
Published online:

[1] A. D. Valentine, T. A. Busbee, J. W. Boley, J. R. Raney, A. Chortos, A. Kotikian, J. D. Berrigan, M. F. Durstock, J. A. Lewis, *Adv. Mater.* **2017**, *29*, 1703817.
[2] a) H. G. Prengel, P. C. Jindal, K. H. Wendt, A. T. Santhanam, P. L. Hegde, R. M. Penich, *Surf. Coat. Technol.* **2001**, *139*, 25; b) K. An, S. Hong, S. Han, H. Lee, J. Yeo, S. H. Ko, *ACS Appl. Mater. Interfaces* **2014**, *6*, 2786.
[3] a) A. Shen, D. Caldwell, A. W. K. Ma, S. Dardona, *Addit. Manuf.* **2018**, *22*, 343; b) W. J. Hyun, S. Lim, B. Y. Ahn, J. A. Lewis, C. D. Frisbie, L. F. Francis, *ACS Appl. Mater. Interfaces* **2015**, *7*, 12619; c) J. Liang, K. Tong, Q. Pei, *Adv. Mater.* **2016**, *28*, 5986.
[4] H. Oh, M. Lee, *Mater. Lett.* **2016**, *176*, 110.
[5] Y. Liu, M. Pharr, G. A. Salvatore, *ACS Nano* **2017**, *11*, 9614.
[6] a) M. Tavakoli, M. H. Malakooti, H. Paisana, Y. Ohm, D. G. Marques, P. Alhais Lopes, A. P. Piedade, A. T. de Almeida, C. Majidi, *Adv. Mater.* **2018**, *30*, 1801852; b) N. Matsuhisa, D. Inoue, P. Zalar, H. Jin, Y. Matsuba, A. Itoh, T. Yokota, D. Hashizume, T. Someya, *Nat. Mater.* **2017**, *16*, 834.
[7] I. Park, S. H. Ko, H. Pan, C. P. Grigoropoulos, A. P. Pisano, J. M. J. Frechet, E. S. Lee, J. H. Jeong, *Adv. Mater.* **2008**, *20*, 489.
[8] T. Yamada, K. Fukuhara, K. Matsuoka, H. Minemawari, J. Tsutsumi, N. Fukuda, K. Aoshima, S. Arai, Y. Makita, H. Kubo, T. Enomoto, T. Togashi, M. Kurihara, T. Hasegawa, *Nat. Commun.* **2016**, *7*, 11402.
[9] a) Y. Son, J. Yeo, H. Moon, T. W. Lim, S. Hong, K. H. Nam, S. Yoo, C. P. Grigoropoulos, D. Y. Yang, S. H. Ko, *Adv. Mater.* **2011**, *23*, 3176; b) S. Kim, W. S. Lee, J. Lee, I. Park, *Nanotechnology* **2012**, *23*, 285301; c) J. Yeo, S. Hong, D. Lee, N. Hotz, M. T. Lee, C. P. Grigoropoulos, S. H. Ko, *PLoS One* **2012**, *7*, e42315; d) E. Tekin, P. J. Smith, U. S. Schubert, *Soft Matter* **2008**, *4*, 703; e) A. Teichler, J. Perelaer, U. S. Schubert, *J. Mater. Chem. C* **2013**, *1*, 1910.
[10] a) D. Herzog, V. Seyda, E. Wycisk, C. Emmelmann, *Acta Mater.* **2016**, *117*, 371; b) D. Wang, Y. Zhang, X. Lu, Z. Ma, C. Xie, Z. Zheng, *Chem. Soc. Rev.* **2018**, *47*, 4611.
[11] a) Y. Ko, J. Kim, D. Kim, Y. Yamauchi, J. H. Kim, J. You, *Sci. Rep.* **2017**, *7*, 2282; b) Z. Zhu, S. Z. Guo, T. Hirdler, C. Eide, X. Fan, J. Tolar, M. C. McAlpine, *Adv. Mater.* **2018**, *30*, 1707495; c) T. Wang, X. Wang, B. Yang, X. Chen, J. Liu, *J. Electrochem. Soc.* **2017**, *164*, D282; d) C. H. Choi, E. Allan-Cole, C. H. Chang, *J. Mater. Chem. C* **2015**, *3*, 7262.
[12] A. J. Kell, C. Paquet, O. Mozenson, I. Djavani-Tabrizi, B. Deore, X. Liu, G. P. Lopinski, R. James, K. Hettak, J. Shaker, A. Momciu, J. Ferrigno, O. Ferrand, J. X. Hu, S. Lafreniere, P. R. L. Malenfant, *ACS Appl. Mater. Interfaces* **2017**, *9*, 17226.
[13] A. Mamidanna, Z. M. Song, C. Lv, C. S. Lefky, H. G. Jiang, O. J. Hildreth, *ACS Appl. Mater. Interfaces* **2016**, *8*, 12594.
[14] Z. Yang, H. Qian, H. Chen, J. N. Anker, *J. Colloid Interface Sci.* **2010**, *352*, 285.
[15] Y. Xia, Y. Xiong, B. Lim, S. E. Skrabalak, *Angew. Chem., Int. Ed.* **2009**, *48*, 60.
[16] A. Kamyshny, S. Magdassi, *Small* **2014**, *10*, 3515.
[17] M. Grouchko, A. Kamyshny, C. F. Mihailescu, D. F. Anghel, S. Magdassi, *ACS Nano* **2011**, *5*, 3354.
[18] Z. Hui, Y. Liu, W. Guo, L. Li, N. Mu, C. Jin, Y. Zhu, P. Peng, *Nanotechnology* **2017**, *28*, 285703.

[19] M. A. Brown, A. Goel, Z. Abbas, *Angew. Chem., Int. Ed.* **2016**, *55*, 3790.
[20] K. Jain, R. Vedarajan, M. Watanabe, M. Ishikiriyama, N. Matsumi, *Polym. Chem.* **2015**, *6*, 6819.
[21] K. Yasuyuki, K. Masayoshi, U. Hirobumi, *J. Micromech. Microeng.* **2015**, *25*, 095002.
[22] Y. Kusaka, K. Nomura, N. Fukuda, H. Ushijima, *J. Micromech. Microeng.* **2015**, *25*, 055022.
[23] D. Jang, D. Kim, B. Lee, S. Kim, M. Kang, D. Min, J. Moon, *Adv. Funct. Mater.* **2008**, *18*, 2862.
[24] L. D. Zarzar, B. S. Swartzentruber, J. C. Harper, D. R. Dunphy, C. J. Brinker, J. Aizenberg, B. Kaehr, *J. Am. Chem. Soc.* **2012**, *134*, 4007.
[25] Z. Zhao, Y. He, H. Yang, X. Qu, X. Lu, J. Luo, *ACS Appl. Mater. Interfaces* **2013**, *5*, 6097.
[26] V. Sunkara, D. K. Park, H. Hwang, R. Chantiwas, S. A. Soper, Y. K. Cho, *Lab Chip* **2011**, *11*, 962.